

Effect of pyridine capping on morphological and optical properties of ZnS:Mn²⁺ core–shell quantum dots

Manju Singhal¹ · J. K. Sharma¹ · H. C. Jeon² · T. W. Kang² · Sunil Kumar²

Received: 22 August 2015 / Accepted: 21 November 2015 / Published online: 28 November 2015
© Springer Science+Business Media New York 2015

Abstract In this work, pyridine-coated ZnS:Mn²⁺ core–shell quantum dots are synthesized through a simple soft chemical route, namely the chemical precipitation method and the effect of pyridine capping has been studied on the morphological and optical parameters of the quantum dots. Morphological properties are investigated through X-ray diffraction (XRD) and transmission electron microscopy. XRD measurements showed that both the ZnS:Mn²⁺ quantum dots and the ZnS quantum dots possessed a zinc blende structure and the crystal structure is not changed with the capping and Mn²⁺ doping. Bandgap measurements are made through UV–visible spectroscopy. FTIR spectra gave the direct evidence that pyridine shells have been successfully coated on the ZnS:Mn²⁺ quantum dots. Room-temperature photoluminescence spectrum of the undoped sample, exhibited only a blue-light emission peaked at 422.6 nm under UV excitation. However, from the Mn²⁺ doped samples, a yellow-orange emission from the Mn²⁺ (⁴T₁ – ⁶A₁) transition has been observed along with the blue emission. For 1 % capping concentration efficient emission of yellow-orange light with the emission peak at 590 nm is observed along with the suppressed defect related blue emission. As pyridine is an excellent capping agent for functionalization of quantum dots by ligand exchange process so the synthesized highly fluorescent core–shell quantum dots are very important for biological applications.

1 Introduction

Quantum dots (QDs) exhibit unique optical and electronic properties that are dependent on a variety of material properties, such as size, shape and composition. Most of the physical or chemical properties exhibited by quantum dots are due to their crystallites. Further growth in their size is due to agglomeration of these crystallites to form primary particles. If this growth of particles is not controlled, they agglomerate and settle down due to Ostwald ripening and Vander–Waals interactions between particles [1, 2]. This agglomeration can be arrested by using capping agents, which adsorbs to the quantum dot surface and prevent agglomeration of the synthesized quantum dots [3, 4]. It has been reported by different researchers that the adequate surface capping concentration can improve the morphological and optical characteristics [2, 5–7]. Thus, core–shell quantum dots are preferred over quantum dots because they show improved and modified properties [8–11]. For example, commercial CdSe quantum dots are generally passivated with ZnS and then coated with a polymer layer that improves their quantum yield and solubility [12]. In terms of biomedical applications, this procedure is ideal for constructing simple fluorescent labels but it can double the nanocrystal diameter and make the CdSe core less accessible to any application. Size is an important consideration in biological applications, where the transport of fluorescent labels across cell walls, cell membranes, and nuclear pores is desired. Also for the initiation of functionalization by ligand exchange process to achieve the desired application, appropriate capping agent is required. Pyridine's hole acceptor behavior is very useful for different kind of ligand exchange processes [13–17]. Capping ligands cover the surface of nanoparticles and controls the solubility of nanocrystals in solution. Since

✉ Sunil Kumar
sunilkumar32@gmail.com

¹ Department of Physics, Maharishi Markandeshwar University, Mullana, Ambala 133 207, India

² Quantum Functional Semiconductor Research Center, Dongguk University, Seoul 100715, South Korea

most of the applications require fluorescent quantum dots, so study of core–shell quantum dots with appropriate dopant is most essential. Transition metal ion dopants added during synthesis significantly contribute to the luminescent properties of these quantum dots. The promising results have motivated the use of these quantum dots in applications ranging from biological sensors to optical displays [18–20].

Different doping materials result in wide range of luminescent properties of the doped materials, which is strongly dependent upon the type of dopant ions. These dopant impurities play a crucial role in changing the electronic structure and transition probabilities of the host material. Zinc sulfide is an important II–VI compound semiconductor having promising applications due to its wide band gap [21–27]. It is also suited for applications in biological systems due to their less toxicity as compared to other II–VI nanoparticles such as CdS, CdTe etc [28, 29]. Owing to the large band gap of ZnS, it can easily host different transition metal ions as luminescent centers [30–33]. As ZnS can be doped with Mn^{2+} very easily and has variety of applications, numerous researchers have investigated the structural and luminescent properties of these nanocrystals [34–40]. According to Bhargava and Gallagher [21], when Mn^{2+} ions are incorporated into the ZnS lattice and substitute for the cation sites, the mixing between the sp electrons of the host ZnS and the d electrons of Mn^{2+} occurs. Thus, forbidden transition of ${}^4\text{T}_1 - {}^6\text{A}_1$ is partially allowed, resulting in the characteristic emission of Mn^{2+} .

As pyridine is a very important capping agent for functionalization of quantum dots by ligand exchange process and keeping in mind the appreciable photoluminescence properties and non-toxic nature of ZnS: Mn^{2+} quantum dots [41–43], in the present study pyridine-capped ZnS: Mn^{2+} quantum dots have been synthesized directly in aqueous solution by chemical precipitation method. Optical and morphological properties of ZnS: Mn^{2+} quantum dots have been studied for different capping concentration of pyridine.

2 Experimental details

Figure 1 presents the flow diagram for the synthesis of pyridine capped ZnS: Mn^{2+} quantum dots. Pyridine capped ZnS: Mn^{2+} quantum dots were synthesized by chemical precipitation method. All the chemicals were of analytical grade and were used without further purification. Homogeneous solutions of zinc acetate, sodium sulfide and manganese acetate were prepared in aqueous media. 0.5 M ($\text{Zn}(\text{CH}_3\text{COO})_2 \cdot \text{H}_2\text{O}$) and 0.5 M Na_2S solutions were used for the synthesis of ZnS quantum

dots. For 1 % Mn^{2+} doping we added 29.75 ml of 0.01 M $\text{Mn}(\text{CH}_3\text{COO})_2 \cdot \text{H}_2\text{O}$ in 49.50 ml solution of 0.5 M ($\text{Zn}(\text{CH}_3\text{COO})_2 \cdot \text{H}_2\text{O}$). Further pyridine (0.01, 0.1, 1.0 and 2.0 At.wt%) was added in zinc acetate solution as a capping agent to the reaction medium for controlling the particle size. After that 0.5 M sodium sulfide was added drop wise. The white precipitate appears soon after the addition of sodium sulfide (Na_2S). The stirring was allowed for 15 min at room temperature using a magnetic stirrer. Then the particles were centrifuged at 4000 rpm for 5 min. The precipitated particles were filtered using Whatman 40 filter paper. The particles were washed several times using double distilled water to remove the last traces of adhered impurities. The washed particles were dried at 60 °C in vacuum oven.

3 Morphological and optical characterization

X-ray diffraction (XRD) studies were done by using Rigaku, model D-max IIIC diffractometer with Cu K_α radiation. TEM studies were conducted using a Transmission Electron Microscope, Hitachi (H-7500) 120 kV equipped with CCD Camera, having a resolution of 0.36 nm (point to point) with 40–120 kV operating voltage and magnification capacity of 6 lakh times in high resolution mode. For TEM studies, the powder was ultrasonicated in ethanol. A drop of this solution was dropped on carbon coated grid. Ethanol was allowed to evaporate and powder remains on grid. Optical absorbance of the ZnS nanoparticles were recorded with a double beam UV–visible spectrophotometer (Model: Hitachi-330) in the range of 200–800 nm. Fourier transform infrared (FTIR) spectra were recorded in range of 4000–400 cm^{-1} with Perkin Spectrum RXI (40). Energy resolved photoluminescence studies were done with Perkin Elmer LS (50B) fluorescence spectrometer.

4 Results and discussion

The nascent ZnS quantum dots and pyridine capped (0.01, 0.1, 1.0, and 2.0 %) ZnS: Mn^{2+} quantum dots were characterized by XRD, TEM, FTIR, UV–visible spectroscopy and energy resolved Photoluminescence spectroscopy.

4.1 X-ray diffraction results

The X-ray diffraction patterns of uncapped ZnS and pyridine capped (0.01 and 2.0 At.wt%) ZnS: Mn^{2+} quantum dots are shown in Fig. 2. All the samples show pure zinc blende crystal structure with the three broad peaks corresponding to the (111), (220) and (311) planes.

Fig. 1 Flow diagram for the synthesis of pyridine capped ZnS:Mn²⁺ quantum dots

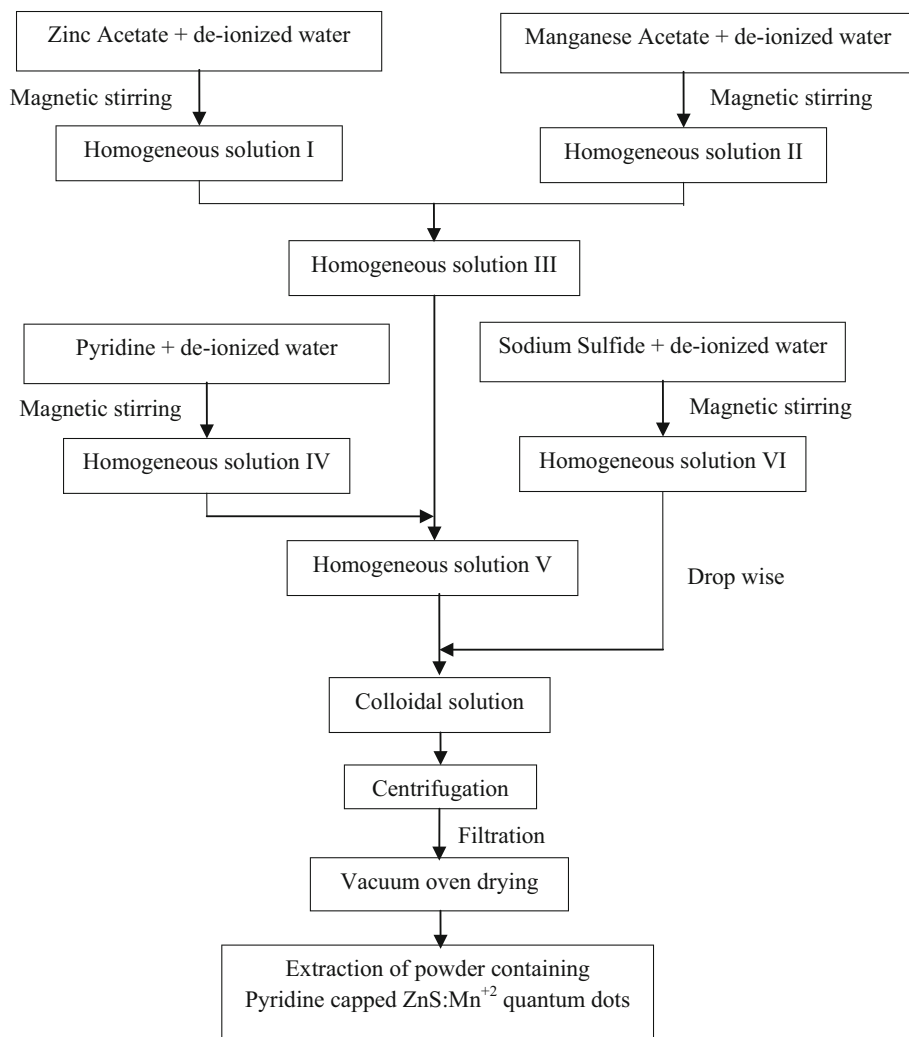
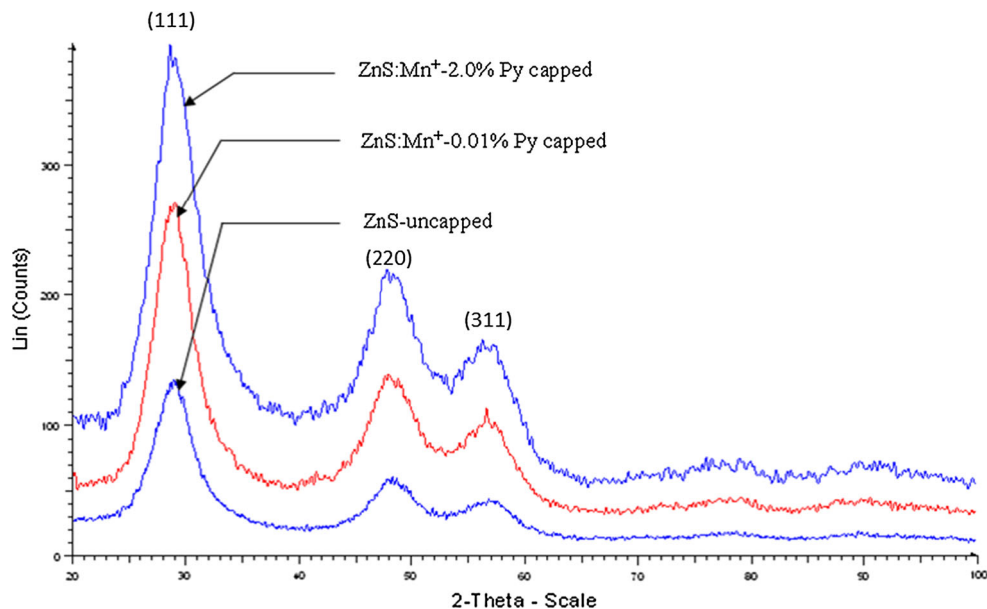


Fig. 2 XRD comparison of uncapped and pyridine capped ZnS:Mn²⁺ quantum dots



The structure of ZnS quantum dots remain unaltered upon doping with the manganese. No diffraction peaks from manganese impurities or any other secondary phase are observed in all the samples. Therefore, it suffices to say that capping and doping did not change the crystal structure of ZnS quantum dots. It is to be noted that the three peaks

observed in the XRD pattern match well with those of the β -ZnS (cubic) reported in the JCPDS Powder Diffraction (File No. 5-0566). Broadening of XRD peaks shows the formation of nanocrystals of ZnS. These nanocrystals have lesser lattice planes compared to bulk, which contributes to the broadening of the peaks in the diffraction pattern. Broad diffraction peaks are attributed to small particle effect [44]. The average crystallite size of all the samples is estimated from the half width of diffraction peaks using Debye–Scherer equation, which is tabulated in the Table 1.

It can be concluded that with increasing capping concentration of pyridine, the crystallite size of ZnS:Mn²⁺ quantum dots decreases with the broadening of XRD peaks.

Table 1 Crystallite size of ZnS:Mn²⁺ pyridine capped quantum dots

Sample	Crystallite size (nm) From (111) peak
Uncapped and undoped ZnS	2.24
0.01 % pyridine capped ZnS:Mn ²⁺	2.04
2.0 % pyridine capped ZnS:Mn ²⁺	1.86

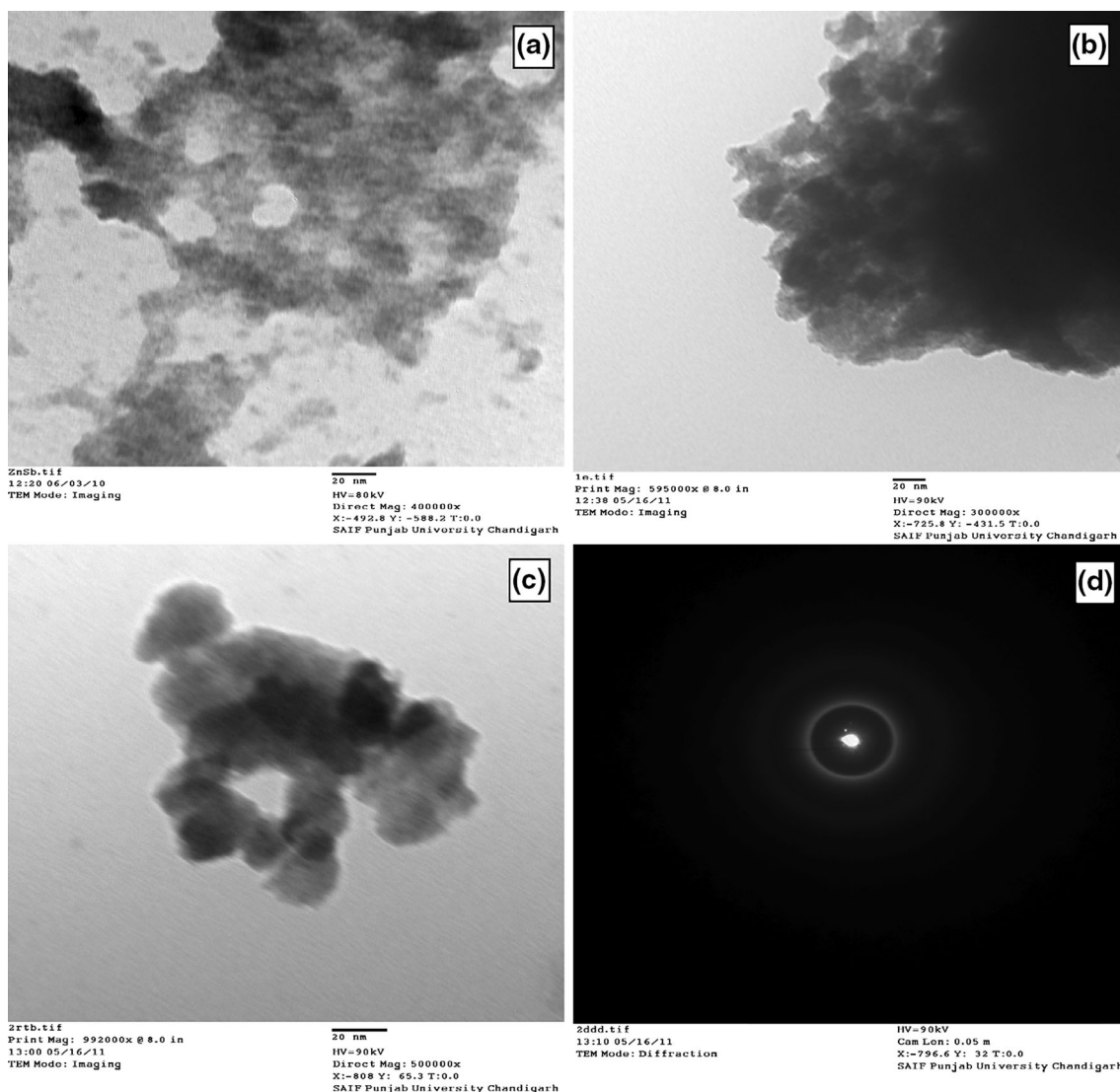


Fig. 3 TEM of **a** uncapped ZnS, **b** 0.01 % pyridine capped ZnS:Mn²⁺, **c** 2.0 % pyridine capped ZnS:Mn²⁺, **d** SAED of pyridine capped ZnS:Mn²⁺ Quantum dots

4.2 Transmission electron microscopy results

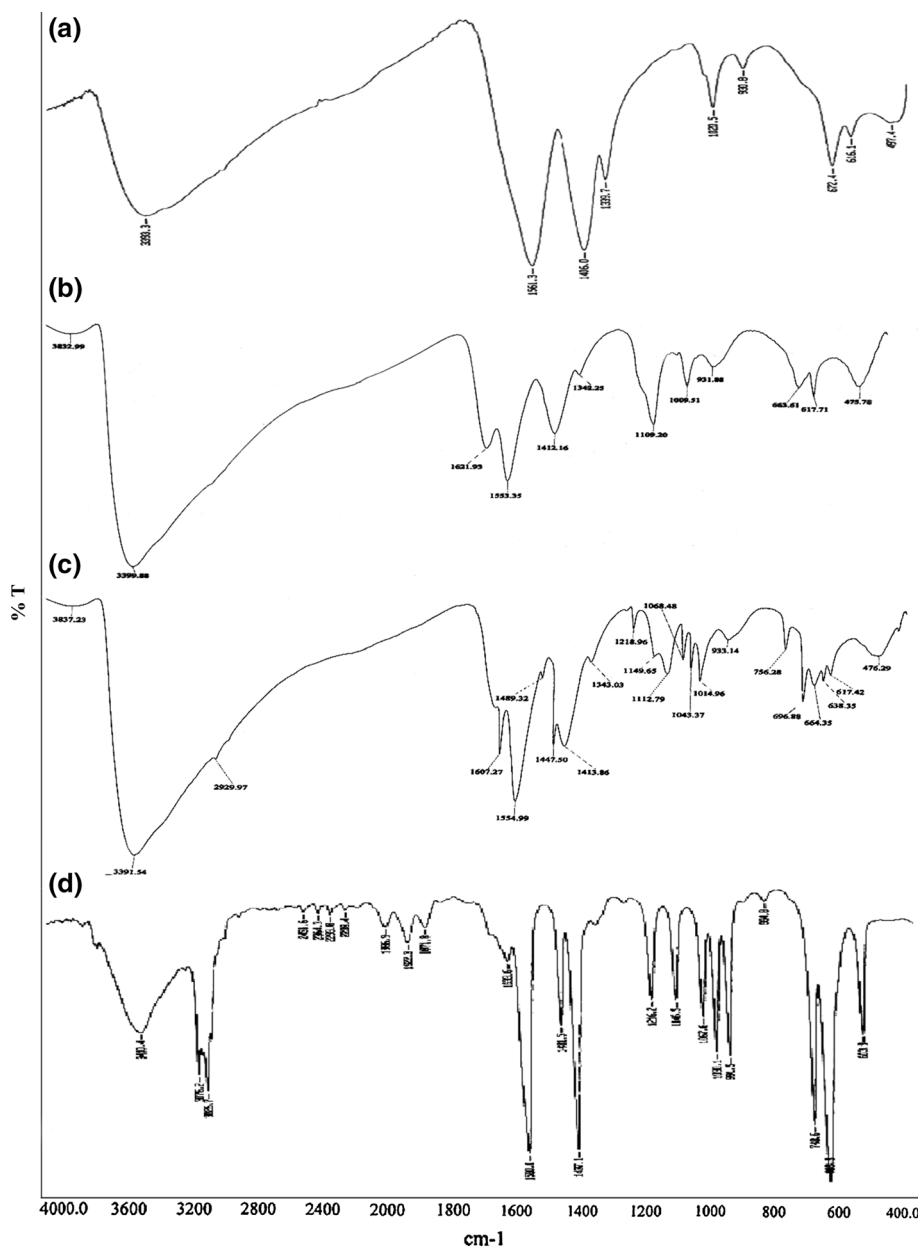
To get the optimum information regarding the morphology of the samples, detailed investigations on the samples have been done by low and high-resolution bright field transmission microscope. Figure 3 shows TEM image of uncapped and capped ZnS:Mn²⁺ nanoparticles. From the TEM micrographs it is clearly observed that uncapped ZnS nanoparticles are agglomerated. TEM images also show that particles are nearly in spherical shape and having average particle size of 2–3 nm. This value is consistent with the XRD result. The selected area diffraction pattern presented, in the Fig. 3d, shows poly-crystallinity of the fabricated quantum dots.

4.3 Fourier transform infrared spectroscopy results

The FTIR scans of uncapped ZnS, pyridine capped ZnS:Mn²⁺ quantum dots and pure pyridine are shown in Fig. 4a–d. There are different features existing between them in the wave number range of 500–4000 cm⁻¹ representing the association of various functional groups. In uncapped ZnS, the bands at 1406 and 1561 cm⁻¹ can be assigned to the symmetric and symmetric stretching of COO⁻ respectively. This shows that the acetate group from the zinc acetate precursor used for zinc ions, have been retained in the synthesized quantum dots.

The broad band at 3393 cm⁻¹ is due to O–H stretching and band at 930 cm⁻¹ due to O–H out of plane bending. Whereas,

Fig. 4 FTIR of **a** uncapped ZnS, **b** 0.01 % pyridine capped ZnS:Mn²⁺, **c** 2.0 % pyridine capped ZnS:Mn²⁺ QDs, **d** pure pyridine



the bands having moderate intensity at 1339 cm^{-1} , may be due to the in-plane C–O–H bending. A moderate intensity band at 1020 cm^{-1} may be due to S–O–C stretching. In the FTIR spectra of pyridine capped ZnS:Mn^{2+} quantum dots absorption peaks in the range $>3000\text{ cm}^{-1}$ is attributed to aromatic =C–H stretch, the strong absorption peaks in the range $1615\text{--}1580\text{ cm}^{-1}$ and $1510\text{--}1450\text{ cm}^{-1}$ are due to the aromatic C=C stretch and absorption peaks in the range $1340\text{--}1250\text{ cm}^{-1}$ is ascribed to aromatic C≡N stretch which this is believed to be due to the formation of co-ordinate bond between the nitrogen atom of pyridine and Zn^{2+} ions. Other small peaks are, however not discussed here. The major peaks at 1559 and 1406 cm^{-1} in the FTIR study strongly support the formation of pyridine capped ZnS:Mn^{2+} quantum dots.

4.4 UV–visible absorption spectroscopy results

Figure 5 shows the absorption spectra of pyridine-encapsulated ZnS:Mn^{2+} and uncapped ZnS quantum dots. The absorption peaks are at 292, 295, 296, 293 and 296 nm for uncapped, 0.01, 0.1, 1.0 and 2.0 % pyridine capped ZnS:Mn^{2+} quantum dots respectively

For obtaining the absorption characteristic of the samples, at first the transmittance (T) at different wavelengths are measured using different values of absorbance and then absorption coefficient (α) at the corresponding wave-lengths are calculated using the Beer–Lambert's relation,

$$\alpha = \frac{1}{d} \ln \left(\frac{1}{T} \right) \quad (1)$$

where d is the path length which is 1 cm in this case.

The relation between the incident photon energy ($h\nu$) and the absorption coefficients (α) is given by the Eq. 2.

$$(\alpha h\nu)^{1/m} = c (h\nu - E_g) \quad (2)$$

where, c is a constant and E_g is the band gap of the material and the exponent m depends on the type of the transition. For direct and allowed transition $m = 1/2$, indirect transition, $m = 2$ and for direct forbidden, $m = 3/2$. For calculating the direct band gap value $(\alpha h\nu)^2$ versus $h\nu$ is plotted as shown in Fig. 6 by extrapolating the straight portion of the graph on $h\nu$ axis at $\alpha = 0$, the optical band gaps are calculated and found to be 3.85, 3.83, 3.85, 3.87 and 3.83 eV respectively for uncapped, 0.01, 0.1, 1.0 and 2.0 % pyridine capped ZnS:Mn^{2+} quantum dots. From the absorption spectra of all samples it is evident that strong quantum confinement effect is observed in all the samples in comparison to the bulk ZnS (3.6 eV).

4.5 Particle size studies

The particle size of pyridine capped Quantum dots was computed using the Brus equation [45]. The average

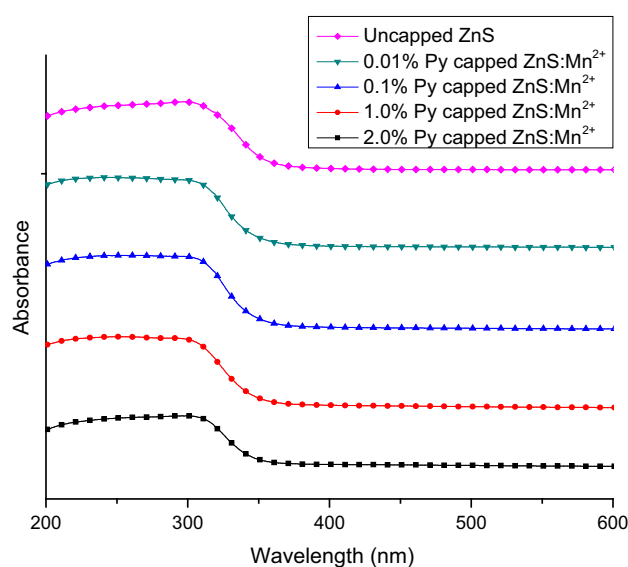


Fig. 5 UV–visible Absorption spectra of uncapped ZnS, 0.01 % pyridine capped ZnS:Mn^{2+} , 0.1 % pyridine capped ZnS:Mn^{2+} , 1.0 % pyridine capped ZnS:Mn^{2+} and 2.0 % pyridine capped ZnS:Mn^{2+} QDs

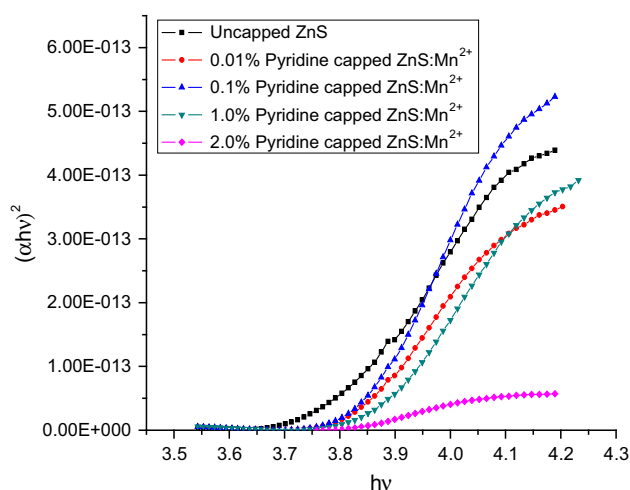


Fig. 6 Band gap comparison of uncapped and pyridine capped ZnS:Mn^{2+} quantum dots

particle size comes out to be 2.72, 2.85, 2.72, 2.61 and 2.85 nm for uncapped, 0.01, 0.1, 1.0 and 2.0 % pyridine capped ZnS:Mn^{2+} quantum dots respectively, which are in accordance with XRD and TEM results. As the Bohr exciton radius in case of ZnS is 5 nm and we are getting average particle size <5 nm. Thus, from our theoretical calculations also, we suggest the observation of quantum confinement effect in case of ZnS.

4.6 Photoluminescence studies

Figure 7 shows the emission spectra of nascent uncapped and 0.01, 0.1, 1.0 and 2.0 % pyridine capped ZnS:Mn^{2+}

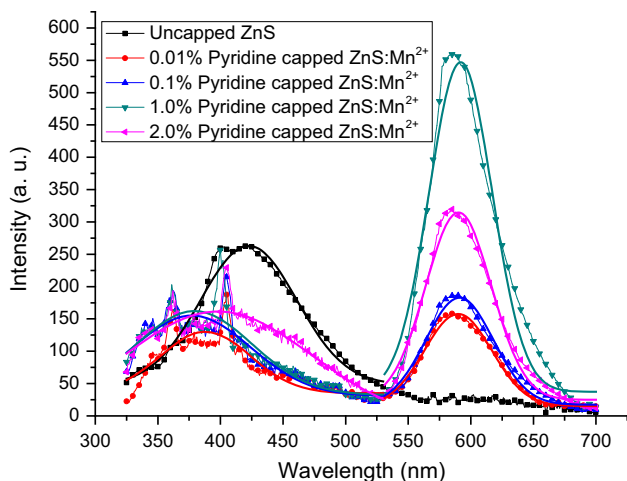


Fig. 7 Photoluminescence emission spectra of the pyridine capped ZnS:Mn²⁺ Quantum dots

Table 2 Data for emission spectra

Sample type	Fixed excitation wavelengths (nm)	Emission peak (nm)
Uncapped	292	422.58
0.01 % capped	295	387.9 and 589.9
0.1 % capped	296	377.1 and 591
1.0 % capped	293	379.2 and 591.9
2.0 % capped	296	398.1 and 590.2

quantum dots, recorded at fixed excitation wavelengths which were taken from the absorption edges of UV–visible spectra. The recorded PL spectra have been smoothed using the Gaussian function of Nonlinear Curve Fit tool in the OriginPro 8[®].

Table 2 shows the emission data for the uncapped and pyridine capped ZnS:Mn²⁺ quantum dots. The photoluminescence spectra of the uncapped ZnS nanoparticles show emission peak at 422.6 nm, which is the characteristic defect related emission of pure ZnS [46]. The photoluminescence spectra of pyridine capped as well as manganese doped ZnS nanoparticles show two emission bands: first defect related blue emission at 387.9, 377.1, 379.2, 398.1 nm and second yellow-orange emission at 589.9, 591.0, 591.9 and 590.2 nm, for 0.01, 0.1, 1.0 and 2.0 % pyridine capped ZnS:Mn²⁺ quantum dots respectively. The blue emission band is associated with the recombination of free charge carriers at defect sites, probably at the surface of nanostructures [47, 48] and the yellow-orange emission at 590 nm can be attributed to the ⁴T₁ – ⁶A₁ transition of the Mn²⁺ impurity [49]. The orange luminescence originates from Mn²⁺ ions on Zn²⁺ sites, where the Mn²⁺ is tetrahedrally coordinated by S²⁻. The characteristics of the Mn²⁺ impurity are almost

identical to the emission observed for Mn²⁺ in bulk ZnS [21, 50, 51]. The intensity of yellow-orange emission first increases with increasing pyridine capping concentration from 0.01 to 1.0 % and then decreases for higher concentration i.e. for 2 %. From the data of emission spectra, it is clear that the intensity of yellow-orange emission is tunable with pyridine capping concentration which is very good for applications like targeted drug delivery, biolabelling and monitoring of controlled drug release rate etc.

5 Conclusion

Nascent and pyridine capped ZnS:Mn²⁺ quantum dots were synthesized with varying capping concentrations through a wet chemical method. Mn doping concentration was selected as 1 % for all the studies because of the optimization of Mn in ZnS is achieved already by our group [52]. The XRD patterns exhibited a zinc blende structure for all the samples. There was no crystalline phase change with manganese and with the increasing pyridine concentration. FTIR studies confirm the capping of ZnS:Mn²⁺ quantum dots with pyridine. Two PL emission bands were observed in ZnS:Mn²⁺ quantum dots which are attributed to the characteristic defect related emission of pure ZnS and ⁴T₁ – ⁶A₁ transition of the Mn²⁺ impurity respectively. Photoluminescence studies reveal that in pyridine capped ZnS:Mn²⁺ quantum dots, Mn²⁺ related yellow-orange emission was observed at 590 nm and intensity of yellow-orange emission increases with increasing the capping concentration of pyridine from 0.01 to 1.0 %, thus emission intensity is tunable with capping concentration which is very novel for biomedical applications.

References

1. J.H. Yao, K.R. Elder, H. Guo, M. Grant, *Phys. Rev. B* **47**, 14110–14125 (1993)
2. H.C. Warad, S.C. Ghosh, B. Hemtanon, C. Thanachayanont, J. Dutta, *Sci. Technol. Adv. Mater.* **6**(3–4), 296–301 (2005)
3. F. Seker, K. Meeker, T.F. Kuech, A.B. Ellis, *Chem. Rev.* **100**, 2505 (2000)
4. M.A. El-Sayed, *Acc. Chem. Res.* **37**, 326–333 (2004)
5. N. Kumbhojkar, V.V. Nikesh, A. Kshirsagar, *J. Appl. Phys.* **88**(11), 6260–6264 (2000)
6. M. Singhal, J.K. Sharma, S. Kumar, *J. Mater. Sci. Mater. Electron.* **23**, 1387–1392 (2012)
7. G. Ghosh, M.K. Naskar, A. Patra, M. Chatterjee, *Opt. Mater.* **28**(8–9), 1047–1053 (2006)
8. J. Lee, V.C. Sundar, J.R. Heine, M.G. Bawendi, K.F. Jensen, *Adv. Mater. Commun.* **12**(5), 1102–1105 (2000)
9. W.J. Parak, D. Gerion, D. Zanchet, A.S. Woerz, T. Pellegrino, C.M. Micheel, S.C. Williams, M. Seitz, R.E. Bruehl, Z. Bryant,

- C. Bustamante, C.R. Bertozzi, A.P. Alivisatos, *Chem. Mater.* **14**(5), 2113–2119 (2002)
10. S. Kumar, M. Singhal, J.K. Sharma, *J. Mater. Sci. Mater. Electron.* **24**, 3875–3880 (2013)
11. W.U. Huynh, J.J. Dittmer, W.C. Libby, G.L. Whiting, A.P. Alivisatos, *Adv. Funct. Mater.* **13**(1), 73–79 (2003)
12. C. Kirchner, T. Liedl, S. Kudera, T. Pellegrino, A. Muñoz Javier, H.E. Gaub, S. Stölzle, N. Fertig, W.J. Parak, *Nano Lett.* **5**, 331–338 (2005)
13. V.I. Klimov, A.A. Mikhailovsky, D.W. McBranch, C.A. Leatherdale, M.G. Bawendi, *Phys. Rev. B.* **61**(20), R13349–R13352 (2000)
14. V.J. Gandubert, R.B. Lennox, *Langmuir* **21**(14), 6532–6539 (2005)
15. S. Rucareanu, V.J. Gandubert, *Chem. Mater.* **18**(19), 4674–4680 (2006)
16. S.J. Wang, H. Kim, H.H. Park, *Vac. Sci. Technol. A.* **28**(4), 559–563 (2010)
17. M. Singhal, J.K. Sharma, S. Kumar, *Adv. Sci. Eng. Med.* **5**(2), 133–139 (2013)
18. Y.Y. Lin, J. Wang, G. Liu, H. Wu, C.M. Wai, Y. Lin, *Biosens. Bioelectron.* **23**(11), 1659–1665 (2008)
19. S.H. Kang, C.K. Kumar, Z. Lee, K.H. Kim, C. Huh, E.T. Kim, *Appl. Phys. Lett.* **93**, 191116–191118 (2008)
20. P. Du, X.Q. Zhang, X.B. Sun, Z.G. Yao, Y.S. Eang, *Chin. Phys. B* **15**, 1370–1373 (2006)
21. R.N. Bhargava, D. Gallagher, *Phys. Rev. Lett.* **72**(3), 416–419 (1994)
22. Z.W. Quan, D.M. Yang, C.X. Li, D.Y. Kong, P.P. Yang, Z.Y. Cheng, J. Lin, *Langmuir* **25**, 10259–10262 (2009)
23. Q.J. Sun, Y.A. Wang, L.S. Li, D.Y. Wang, T. Zhu, J. Xu, C.H. Yang, Y.F. Li, *Nat. Photonics* **1**, 717–722 (2007)
24. Y. Yang, Y.Q. Li, S.Y. Fu, H.M. Xiao, *J. Phys. Chem. C* **112**, 10553–10558 (2008)
25. K. Manzoor, S.R. Vadera, N. Kumar, T.R.N. Kutty, *Appl. Phys. Lett.* **84**(2), 284–286 (2004)
26. A. Vecht, *J. Cryst. Growth* **59**, 81–97 (1982)
27. Y. Yang, S. Xue, S. Liu, J. Huang, J. Shen, *Appl. Phys. Lett.* **69**, 377–379 (1996)
28. J.P. Li, Y. Xu, Y. Liu, D. Wu, Y. Sun, *China Particulol.* **2**, 266–269 (2004)
29. Y. Li, J. Chen, C. Zhu, L. Wang, D. Zhao, S. Zhao, Y. Wu, *Spectrochim. Acta Part A* **60**, 1719–1724 (2004)
30. M. Wang, L. Sun, X. Fu, C. Liao, C. Yan, *Solid State Commun.* **115**(9), 493–496 (2000)
31. A.A. Bol, J. Ferwerda, J.A. Bergwerff, A. Meijerink, *J. Lumin.* **99**, 325–334 (2002)
32. H. Soni, M. Chawda, D. Bodas, *Mater. Lett.* **63**(9), 767–769 (2009)
33. A.A. Bol, R.V. Beek, A. Meijerink, *Chem. Mater.* **14**(3), 1121–1126 (2002)
34. D. Denzler, M. Olschewski, K. Sattler, *J. Appl. Phys.* **84**(5), 2841–2845 (1998)
35. A.A. Ashkarran, *Mater. Sci. Semicond. Process.* **17**, 1–6 (2014)
36. S. Sen, C.S. Solanki, P. Sharma, *J. Lumin.* **145**, 669–675 (2014)
37. R.N. Bhargava, *J. Lumin.* **70**(1–6), 85–94 (1996)
38. N. Karar, F. Singh, B.R. Mehta, *J. Appl. Phys.* **95**, 656–660 (2004)
39. Y. Ding, X.D. Wang, Z.L. Wang, *Chem. Phys. Lett.* **398**, 32–36 (2004)
40. A.B. Cruz, Q. Shen, T. Toyoda, *Mater. Sci. Eng. C* **25**, 761–765 (2005)
41. H.F. Wang, Y. He, T.R. Ji, X.P. Yan, *Anal. Chem.* **81**(4), 1615–1621 (2009)
42. H.F. Wang, Y. Li, Y.Y. Wu, Y. He, X.P. Yan, *Chem. Eur. J.* **16**, 12988–12994 (2010)
43. P. Wu, Y. He, H.F. Wang, X.P. Yan, *Anal. Chem.* **82**(4), 1427–1433 (2010)
44. S.B. Qadri, E.F. Skelton, D. Hsu, A.D. Dinsmore, J. Yang, H.F. Gray, B.R. Ratna, *Phys. Rev. B* **60**(13), 9191–9193 (1999)
45. L.E. Brus, *J. Chem. Phys.* **80**, 4403–4409 (1984)
46. M. Sharma, S. Kumar, O.P. Pandey, *J. Nanopart. Res.* **12**, 2655–2666 (2010)
47. A.A. Bol, A. Meijerink, *Phys. Rev. B* **58**(24), 15997–16000 (1998)
48. S. Kar, S. Chaudhary, *J. Phys. Chem. B* **109**(8), 3298–3302 (2005)
49. B. Xia, I.W. Lenggoro, K. Okuyama, *Chem. Mater.* **14**, 4969–4974 (2002)
50. A.A. Bol, A. Meijerink, *J. Lumin.* **87**, 315–318 (2000)
51. H.S. Bhatti, R. Sharma, N.K. Verma, *Parmana. J. Phys.* **65**(3), 541–546 (2005)
52. A. Jain, S. Panwar, T.W. Kang, H.C. Jeon, S. Kumar, R.K. Choubey, *J. Mater. Sci. Mater. Electron.* **25**(4), 1716–1723 (2014)